Qualitative Improvement of Z_{eff} Diagnostic Based on Visible Bremsstrahlung Profile Measurement by Changing Observation Cross Section in LHD*)

Yasuko KAWAMOTO[1)], Shigeru MORITA[1)], Motoshi GOTO[1,2)] and Tetsutarou OISHI[1,2)]

[1)]*National Institute for Fusion Science, Toki, Gifu 509-5292, Japan*

[2)]*The Graduate University for Advanced Studies, SOKENDAI, Toki, Gifu 509-5292, Japan*

(Received 26 November 2020 / Accepted 17 February 2021)

Full vertical profiles of visible bremsstrahlung continuum have been measured for diagnostics of effective ion charge, Z_{eff}, with parallel optical fiber arrays at horizontally elongated plasma cross section in the Large Helical Device (LHD). Measured bremsstrahlung profiles were asymmetric due to non-uniform bremsstrahlung emissions located in the stochastic magnetic field layer. Then, the Z_{eff} profile analysis has been done only for a magnetic configuration with relatively thin stochastic magnetic field layer, i.e. for plasmas at magnetic axis position of $R_{ax} = 3.60$ m. The effect of the non-uniform bremsstrahlung emission disappears in the lower half profile at $R_{ax} = 3.60$ m, while the Z_{eff} profile analysis is extremely difficult in other magnetic configurations due to the presence of the non-uniform bremsstrahlung emission over the entire vertical profile from top to bottom. To improve the difficult situation in the Z_{eff} diagnostic the fan array optical fiber system was newly installed at vertically elongated plasma cross section for full horizontal profile measurement. It is found that the non-uniform bremsstrahlung emissions disappear from the signal and the observed bremsstrahlung profile is almost symmetric between inboard and outboard radial profiles. The analysis on the Z_{eff} profile has been carried out based on the plasma equilibrium database in LHD, TSMAP. A preliminary result is obtained in high-density discharges, which shows a flat Z_{eff} profile and values of $Z_{eff} \sim 1$.

Keywords: effective ion charge, bremsstrahlung, visible spectrometer, Large Helical Device

DOI: 10.1585/pfr.16.2402072

1. Introduction

The effective ion charge, Z_{eff}, is one of the most important plasma parameters in fusion research. Because the collisionality of plasma particles depends on the value of Z_{eff}, the Z_{eff} diagnostic becomes important in studying the transport in toroidal devices. The Z_{eff} value is additionally important in tokamaks because the ohmic input power and the plasma current directly depends on the toroidal plasma resistivity as a function of the Z_{eff}. On the other hand, the value of Z_{eff} indicates an impurity ion density. As the density of heavy impurities is considerably low in fusion plasmas, e.g. $n_{imp}/n_e < 10^{-4}$, the Z_{eff} value generally suggests the ion density of light impurities. Therefore, the Z_{eff} value can be an index of the fuel dilution, which results in a reduction of the fusion energy output.

In general, the value of Z_{eff} is measured from intensity of the bremsstrahlung continuum. Because the bremsstrahlung continuum intensity at high-energy range such as x-ray region has a strong temperature dependence and involves contribution of the recombination continuum originated in highly ionized impurity ions, which leads to an apparent increase in the bremsstrahlung intensity. This is a main reason why the visible bremsstrahlung continuum is widely used for the Z_{eff} diagnostic in fusion research [1]. Then, the visible bremsstrahlung continuum has been also measured in LHD to evaluate the Z_{eff} profile.

In LHD, at first, a vertical profile of the visible bremsstrahlung continuum was measured at horizontally elongated plasma cross section in combination with photomultiplier tubes, an interference filter with central transmission wavelength of 530 nm and parallel optical fiber array mainly to study the impurity transport [2]. However, measured bremsstrahlung profiles showed an asymmetric profile in all magnetic configurations except for the lower half profile at magnetic axis position of $R_{ax} = 3.60$ m with thin stochastic magnetic field layer. At this point, we believed the reason why the bremsstrahlung profile is asymmetric originated in mixture of impurity line emissions existing near 530 nm into the bremsstrahlung signal.

Next, a visible spectrometer system was installed on the same diagnostic port to measure only the bremsstrahlung continuum, excluding the contribution of impurity line emissions. Unfortunately, contrary to our expectations, the visible bremsstrahlung profile measured with the spectrometer system also indicated an asymmet-

author's e-mail: kawamoto.yasuko@nifs.ac.jp

*) This article is based on the presentation at the 29th International Toki Conference on Plasma and Fusion Research (ITC29).

ric profile as described later [3]. The result was basically the same as that from the interference filter system, while the Z_{eff} profile has been analyzed using the lower half bremsstrahlung profile at $R_{ax} = 3.60$ m configuration. Thus, we found that the asymmetric bremsstrahlung profile was caused by non-uniform bremsstrahlung emissions from the stochastic magnetic field layer located outside the core plasma [4].

In order to examine the effect of non-uniform bremsstrahlung emissions, an optical fiber array has been recently installed on another diagnostic port from which a horizontal profile at vertically elongated plasma cross section can be observed. Surprisingly, the bremsstrahlung profile measured at the vertically elongated plasma cross section was entirely different from that at the horizontally elongated plasma cross section. We observed almost symmetric bremsstrahlung profile for the first time. This report describes the first result on the observation of entirely different bremsstrahlung profiles between the horizontally and the vertically elongated plasma cross sections in LHD. A preliminary result on Z_{eff} analysis from the symmetric bremsstrahlung profile is also shown.

2. Principle of Z_{eff} Evaluation

The value of Z_{eff} is evaluated from the bremsstrahlung continuum emissivity $\varepsilon^{B}(\lambda, n_e, T_e)\,[Wm^{-3}\,m^{-1}]$ which is emitted through the acceleration of electrons based on the Coulomb collision with plasma ions. The bremsstrahlung emissivity is expressed as functions of wavelength, λ, electron density, n_e, and temperature, T_e, in the following equation;

$$\varepsilon^{B}(\lambda, n_e, T_e) = Z_{eff} \times \frac{2^6\sqrt{2}}{3\sqrt{3}} \frac{\pi^{1/2}\alpha h a_0^2 R^2}{m^{3/2} c} \sqrt{\frac{1}{kT_e}} \times \exp\left(-\frac{hc/\lambda}{kT_e}\right) < g_{ff}(T_e, \lambda) > n_e^2 \frac{1}{\lambda^2}, \quad (1)$$

where α, $h\,[J \cdot s]$, $a_0\,[m]$, $R\,[J]$, $m\,[kg]$ and $c\,[m/s]$ are the fine structure constant, Planck's constant, Bohr radius, Rydberg constant, the electron mass and the light speed, respectively. The value of $\langle g_{ff}(T_e, \lambda)\rangle$ means the velocity-averaged Gaunt factor for free-free transitions [5]. Here, the bremsstrahlung intensity, $I^{B}(\lambda_0, n_e, T_e)\,[Wm^{-2}]$, at certain wavelength, λ_0, is obtained by integrating the local emission within the last closed flux surface along the line-of-sight (LOS). The intensity is then defined by

$$I^{B}(\lambda_0, n_e, T_e) = \int^{\mathrm{LOS}} \varepsilon^{B}(\lambda_0, n_e, T_e)\,dl. \quad (2)$$

Thus, the line-averaged Z_{eff} can be defined as $\langle Z_{eff}\rangle$ with a ratio of the measured bremsstrahlung intensity, I^{B}_{mes}, to the calculated bremsstrahlung intensity in a pure hydrogen plasma, I^{B}_{cal}, at $Z_{eff} = 1$. The equation is simply expressed by

$$\langle Z_{eff}\rangle = \frac{I^{B}_{mes}(\lambda_0, T_e, n_e)}{I^{B}_{cal}(\lambda_0, T_e, n_e)}. \quad (3)$$

The denominator can be easily calculated as the sum of the local bremsstrahlung intensity, i.e., product of the local bremsstrahlung emissivity and length along the LOS between adjacent two magnetic surfaces.

3. Experimental Setup

A compact Czerny-Turner visible spectrometer with focal length of 300 mm (Model: MK-300, Bunkokeiki co. Ltd.), of which the astigmatism is corrected by installing additional toroidal mirror, has been used for the bremsstrahlung profile measurement. The spectrometer with 100 µm core diameter optical fibers was originally installed on #10-O port at horizontally elongated plasma cross section (see Fig. 1 (a)). For the present study, the spectrometer system has moved to #7.5-L port, from which the radial profile at vertically elongated plasma cross section can be observed. A fan array type optical fiber system was newly installed as seen in Fig. 1 (b). The fan array has a sufficient poloidal spread angle of 18° to cover the full range of the plasma cross section. A low-resolution grating with 300 grooves/mm (spectral resolution: $\Delta\lambda = 1.71$ nm)

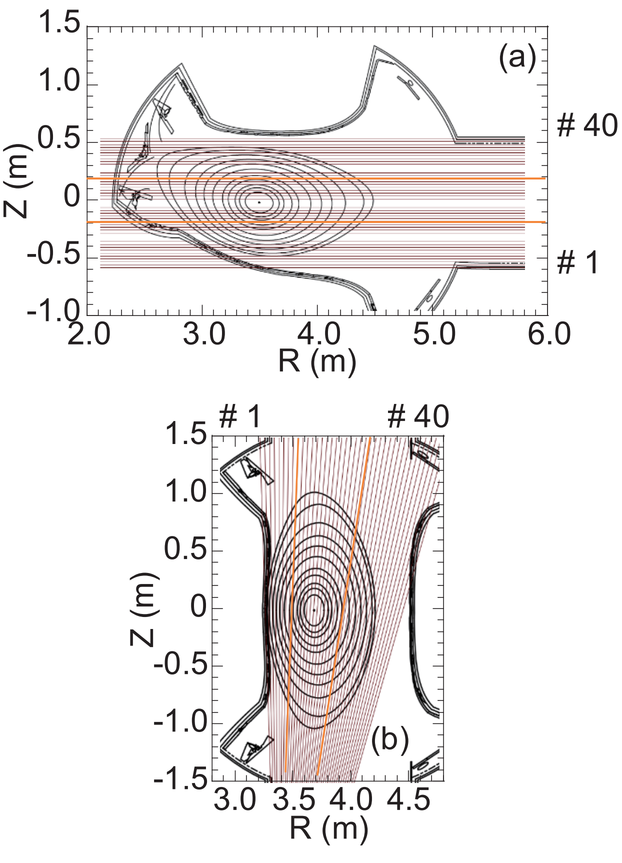

Fig. 1 Viewing chords with 40 optical fibers at (a) horizontally elongated plasma cross section (#10-O port) and (b) vertically elongated plasma cross section (#7.5-L port). Magnetic surfaces are plotted for $R_{ax} = 3.60$ m configurations. Two orange thick solid lines in (a) indicate the viewing chords at $Z = -0.195$ m and -0.195 m and those in (b) indicate the viewing chords at $R = 3.51$ m and 3.98 m.

is normally selected from pre-installed three gratings to increase the spectrometer throughput because the visible bremsstrahlung intensity is weak. When the spectral lines are identified in details, a high-resolution grating with 1200 grooves/mm ($\Delta\lambda = 0.39$ nm) is selected. A charge-coupled detector (CCD) with 1024×1024 pixels and pixel size of $13 \times 13\,\mu\mathrm{m}^2$ (Andor DU-934N) is equipped to observe the focal image. The time resolution per single image frame, which is adjustable by using the sub-image operation mode, is set to 100 ms in the present measurement.

In order to measure the bremsstrahlung profile simultaneously at two different plasma cross sections, another Czerny-Turner astigmatism-corrected visible spectrometer with focal length of 500 mm (Model: Chromex 500is, Bruker Optics, Inc.,: $\Delta\lambda = 2.34$ nm) was used to observe the vertical profile in range of $-0.58\,\mathrm{m} < Z < 0.58\,\mathrm{m}$ at horizontally elongated plasma cross section, as shown in Fig. 1 (a). For the purpose, 40 parallel viewing chords are set on the #10-O port. The viewing chord is tilted slightly by an angle of 6° from the direction perpendicular to the toroidal magnetic field. As the focal length is relatively long and the angle of incidence of visible light on the grating is close to a normal incidence in this spectrometer system, the system throughput is considerably low in comparison with the MK-300 spectrometer. Then, a low-resolution grating with 100 grooves/mm is used in the present measurement to increase the throughput. As a result, a wide spectral wavelength range (> 300 nm) can be simultaneously observed because the reciprocal linear dispersion is large, 20 nm/mm. The CCD detector with 1024×255 pixels and pixel size of $26 \times 26\,\mu\mathrm{m}^2$ (Andor DV420) is also used in this spectrometer. The CCD is normally operated at cooling temperature of −20°C and the data is taken at every 200 ms. Both spectrometers are placed in an underground room to avoid signal noise and detector damage due to neutrons and γ-rays during deuterium discharges.

4. Results and Discussions

Typical visible spectra measured at $400 \le \lambda \le 750$ nm in $R_{ax} = 3.60$ m configuration are plotted in Fig. 2 with solid line. Figures 2 (a) and (b) show the spectrum observed at $Z = 0.195$ m and $Z = -0.195$ m in the horizontally elongated plasma cross section, respectively (see Fig. 1 (a)). In Fig. 2 the radial position where the bremsstrahlung intensity takes the maximum value is chosen in plotting the two spectra to make clear the difference. In Fig. 2 (a) several impurity lines with strong intensities are emitted from the stochastic magnetic field layer where low-ionized impurity ions stay. It is clear that the edge impurity content near the inboard divertor is locally enhanced even in the magnetic configuration with thinner stochastic magnetic field layer such as $R_{ax} = 3.60$ m. It should be noted here that the edge impurity line emissions are strong across all vertical areas in the magnetic configurations with thicker stochastic magnetic field layer, e.g. $R_{ax} \ge 3.75$ m.

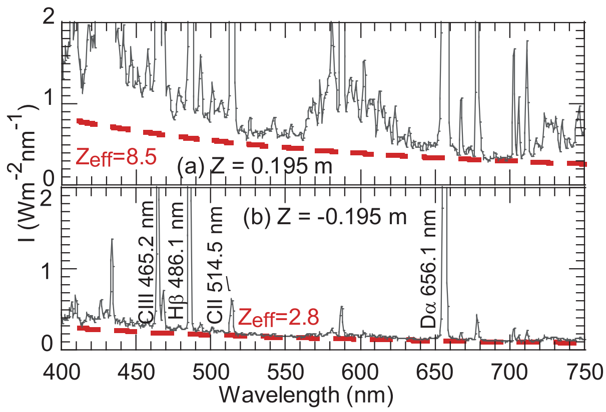

Fig. 2 Examples of visible spectrum measured from #10-O port (solid lines) at (a) $Z = 0.195$m and (b) $Z = -0.195$ m. The spectra are with 100 grooves/mm grating. Synthetic bremsstrahlung spectrum from 400 nm to 750 nm is shown with dashed lines.

The dashed lines in the figure represent the calculated bremsstrahlung intensity of which the absolute value is determined by fitting the measured spectra. A spatially constant Z_{eff} profile is assumed to calculate the synthetic bremsstrahlung intensity along the viewing chord based on the Eq. 2. Here, T_e and n_e profiles measured with Thomson scattering diagnostic are reconstructed into a function of normalized radius, ρ is r_{eff}/a_{max}, where r_{eff} is effective plasma radius and a_{max} is the closed magnetic field of plasma radius, based on the plasma equilibrium calculation code, TSMAP [6]. The Z_{eff} value at $Z = 0.195$ m in Fig. 2 (a) is as a result too large, while the value is reasonable at $Z = -0.195$ m in Fig. 2 (b).

The bremsstrahlung continuum intensity measured at 530 nm is plotted in Figs. 3 (a) and (b) for observations at horizontally (#7.5-L port) and vertically (#10-O port) elongated plasma cross sections, respectively as a function of vertical (Z) and horizontal (R) positions, respectively. The data are simultaneously taken from the same discharge ($R_{ax} = 3.60$ m and $B_t = 2.75$ T) with high density of $7.5 \times 10^{19}\,\mathrm{m}^{-3}$. All bremsstrahlung intensities in the figures are obtained through the same manner as the analysis in Fig. 2. Therefore, the radial bremsstrahlung profiles in Fig. 3 do not include any contribution from impurity line emissions.

The radial bremsstrahlung profile at horizontally elongated plasma cross section in Fig. 3 (a) indicates an entire asymmetric profile. The intensity unreasonably increases in the upper-half profile, in particular, at around $Z = 0.19$ m. We believe that the asymmetric profile is caused by a non-uniform electron and/or impurity density distribution in the stochastic magnetic field layer. The non-uniform bremsstrahlung profile will be studied as our future work in relation to the structure of the stochastic magnetic field layer, in particular, at the inboard side. On the contrary, in the case of vertically elongated plasma cross

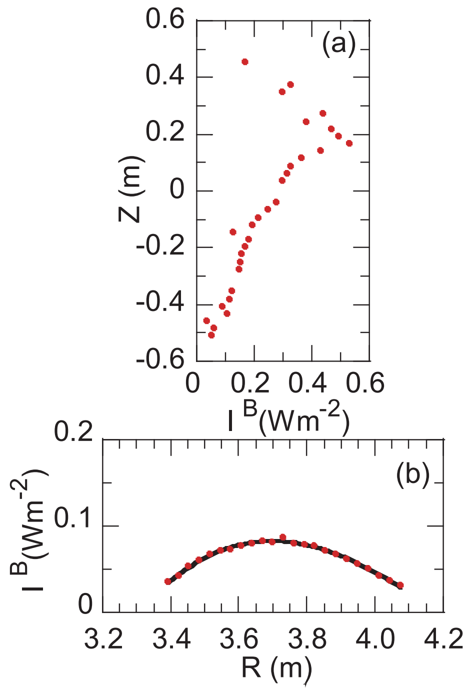

Fig. 3 Intensity of bremsstrahlung continuum at 530 nm obtained at (a) 10-O and (b) 7.5-L ports (#159146). Solid line in (b) indicates a fitting curve with cubic polynomial function.

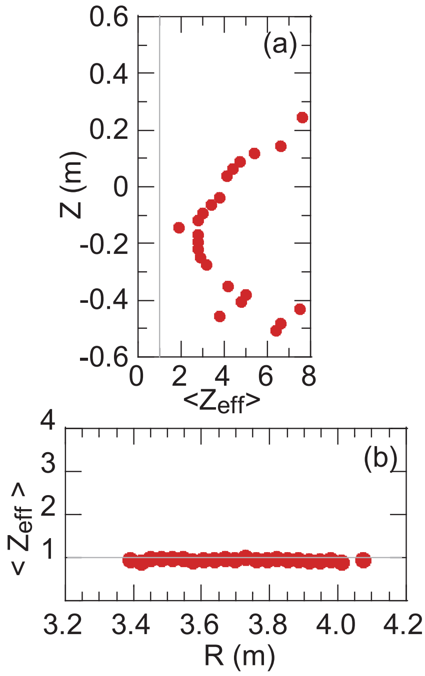

Fig. 4 Radial profiles of line-averaged Z_{eff}, $\langle Z_{eff} \rangle$ at (a) #10-O and (b) #7.5-L ports (#159146).

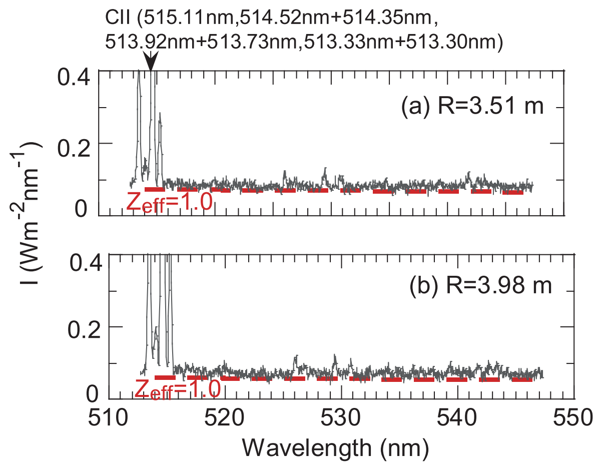

Fig. 5 Examples of enlarged visible spectrum at (a) $R = 3.51$ m and (b) 3.98 m measured from #7.5-L port (#159146). The spectra are measured with 1200 grooves/mm. Synthetic bremsstrahlung spectrum calculated from 510 nm to 550 nm is shown with dashed lines.

section in Fig. 3 (b), an almost symmetric bremsstrahlung profile is obtained. That the peak position in the radial profile moved to $R = 3.7$ m indicates an effect of the plasma axis shift due to the plasma pressure which changes the radial structure of magnetic surfaces. As a result, the viewing chord length passing through the plasma center at vacuum condition of $R_{ax} = 3.60$ m becomes shorter, which leads to a reduction of the measured bremsstrahlung intensity. We notice here that the magnetic surfaces plotted in Fig. 1 show the contours at the vacuum condition. The radial intensities in Fig. 3 (b) are fitted with a cubic polynomial function to reconstruct into the local emissivity profile. As the data at the plasma edge, i.e., $R < 3.4$ m and $R \geq 4.1$ m, are scattered, the present analysis is done using the data from plasma core region, i.e., $3.4 \leq R < 4.1$ m.

The line-averaged Z_{eff} analyzed from Fig. 3 based on Eq. 3 is shown in Fig. 4. As a matter of course, the radial profile of $\langle Z_{eff} \rangle$ at #10-O port becomes extremely asymmetric and the values of $\langle Z_{eff} \rangle$ are unreasonably large. On the other hand, the $\langle Z_{eff} \rangle$ values at #7.5-L port distribute around unity showing a flat radial profile. As the density is considerably high in the discharge, the $\langle Z_{eff} \rangle$ values obtained at #7.5-L port are quite reasonable.

The visible spectra near 530 nm are observed using a high-resolution grating, i.e., 1200 groove/mm, to examine the presence of impurity lines and the bremsstrahlung continuum intensity in details. The results are shown in Fig. 5. Figures 5 (a) and (b) indicate the visible spectrum in range of $510 \leq \lambda \leq 550$ nm for viewing chords passing through $R = 3.51$ m and 3.98 m positions at $Z = 0$ m, respectively. In this wavelength range, there is no strong impurity line except for CII lines at wavelength range of $\lambda < 516$ nm, and a sufficient intensity of the bremsstrahlung continuum can be observed in the spectra. Then, it is very clear that the impurity line emission does not affect the present bremsstrahlung continuum analysis, at least in the observation from vertically elongated plasma cross section at #7.5-L port.

A preliminary analysis on the Z_{eff} profile is carried out based on the result from vertically elongated plasma cross

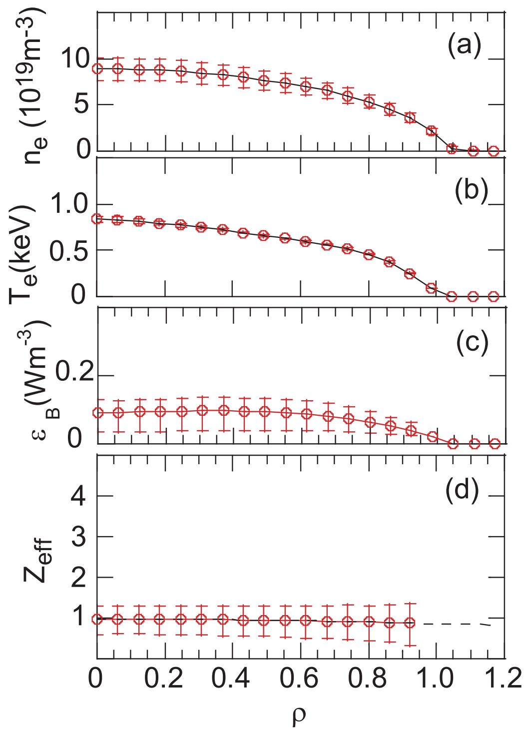

Fig. 6 Radial profile of (a) electron density, (b) electron temperature, (c) bremsstrahlung emissivity, (d) Z_{eff} as a function of averaged plasma radius, ρ (= r_{eff}/a_{max}) (#159146).

section shown in Figs. 3 - 4. The result of the Z_{eff} analysis is shown in Fig. 6. Figures 6 (a) and (b) indicate radial profiles of electron density and temperature. The magnetic surface structure reformed by the finite β-effect is taken into account in the data analysis based on the TSMAP code. The local emissivity profile of the bremsstrahlung is reconstructed from the fitting profile of measured intensities shown in Fig. 3 (b). The result is plotted in Fig. 6 (c). It should be noticed that the obtained bremsstrahlung emissivity profile is quite similar to the electron density profile in Fig. 6 (a). Thus, the Z_{eff} profile is obtained from Eq. (1), as shown in Fig. 6 (d). The profile is considerably flat. The error in analyzing the Z_{eff} profile mainly originates in the error bars of electron densities from Thomson scattering diagnostic. Since the photon energy of the visible bremsstrahlung continuum is very small, i.e., a few eV, compared to the electron temperature, the effect of the electron temperature against the Z_{eff} analysis may be ignored.

5. Summary

The Z_{eff} profile diagnostic was qualitatively improved by changing the observed plasma cross section from #10-O port with horizontal viewing chords to #7.5-L port with vertical viewing chords. A simultaneous measurement of the bremsstrahlung profile at the #10-O and #7.5-L ports indicated a clear difference of asymmetric and symmetric profiles. Since the bremsstrahlung signal obtained from the spectrometer has no sufficient contribution of impurity line emissions, the asymmetric bremsstrahlung profile observed at upper half of the horizontally elongated plasma cross section at #10-O port might be due to the non-uniform density distribution in the stochastic magnetic field layer. That fact suggests that a stagnation region surrounded by magnetic fields, which locates at inboard side of the horizontally elongated plasma cross section, maintains a high-density plasma. The investigation for the cause of why the bremsstrahlung profile becomes extremely asymmetric of the non-uniform bremsstrahlung distribution is very important in addition to the further development of the Z_{eff} diagnostic.

Acknowledgements

This work was partly supported by NIFS project financial support (No. NIFS19ULPP010) and Grant-in-Aid for Scientific Research No. 20K15208 and 16H04088. The authors thank Profs. M. Osakabe and T. Morisaki for their continuous supports to this study.

[1] K. Kadota *et al.*, Nucl. Fusion **20**, 209 (1980).
[2] H. Nozato *et al.*, J. Plasma Fusion Res. **5**, 442 (2002).
[3] H.Y. Zhou *et al.*, J. Appl. Phys. **107**, 053306 (2010).
[4] H.Y. Zhou *et al.*, Rev. Sci. Instrum. **81**, 10D706 (2010).
[5] P.J. Story and D.G. Hummer, Comput. Phys. Commun. **66**, 129 (1991).
[6] M. Emoto *et al.*, Fusion Eng. Des. **87**, 2076 (2012).